SCALE-DEPENDENT ANALYSIS OF CURVATURE AND TORSION STATISTICS IN HOMOGENEOUS TURBULENT SHEAR FLOW

Frank G. Jacobitz
Department of Mechanical Engineering, University of San Diego
5998 Alcalá Park, San Diego, California 92110, USA
jacobitz@sandiego.edu

Kai Schneider
Institut de Mathématiques de Marseille (I2M), Aix-Marseille Université, CNRS
3 place Victor Hugo, case 19, 13331 Marseille Cedex 3, France
kai.schneider@univ-amu.fr

ABSTRACT

Direct numerical simulation results of homogeneous turbulent shear flow representing Saffman turbulence are evaluated in order to study scale-dependent curvature and torsion statistics. The statistics are computed using volume averages at a given time in the flow evolution and previously reported scaling laws determined along Lagrangian particle paths are obtained. Using a wavelet-based, scale-dependent decomposition of the velocity field, probability density functions (pdfs) of the curvature vector component magnitude are determined at different scales of the turbulent motion. While the component pdfs collapse in the case of isotropic turbulence, they differ for small values of the curvature in the case of anisotropic homogeneous turbulent shear flow. Their anisotropy directly follows the diagonal components of the Reynolds stress anisotropy tensor. This indicates the causal effect of large-scale, coherent vortices on the geometrical statistics of fluid particle paths.

INTRODUCTION

Analyzing curvature and torsion in turbulent flows allows for a better understanding of the geometry and dynamics of fluid particle motions. These Lagrangian descriptors provide a more nuanced perspective than traditional Eulerian statistics, as they capture the localized history of a particle's interaction with the surrounding flow field (Yeung, 2002; Toschi & Bodenschatz, 2009). Curvature and torsion provide insights into the structure and behavior of turbulent eddies, vortex filaments, and other coherent structures that define the complex topology of the flow field. These geometric properties are particularly sensitive to small-scale intermittency. For example, extreme events in curvature are often associated with the high-intensity vorticity found in the cores of dissipative structures (Braun *et al.*, 2006; Xu *et al.*, 2007).

A robust characterization of these effects is crucial for accurate modeling and design in both industrial and environmental systems. In engineering, curvature statistics are essential for refining Lagrangian stochastic models used to predict pollutant dispersion, particle deposition, and mixing efficiency (Pope, 1994; Minier & Peirano, 2001; Duplat & Villermaux, 2008). Furthermore, in geophysical flows, such as those found in the atmospheric boundary layer or oceanic currents, the twisting motion of trajectories influences the transport of nutrients and heat (LaCasce, 2008; Franzese, 2003). In the specific context of sheared turbulence, the work of Jacobitz *et al.* (2016); Jacobitz & Schneider (2021) utilizing direct numerical simulations demonstrates how mean shear and stratification modulate the probability density functions of Lagrangian accelerations, which are directly tied to a trajectory's curvature and torsion. Understanding these geometric quantities under anisotropic conditions is vital for improving large eddy simulations, where subgrid-scale motions must be accurately parameterized to predict macro-scale transport in complex industrial and geophysical environments (Meneveau & Katz, 2000).

This study considers curvature and torsion statistics in homogeneous turbulent shear flow. These quantities were computed from the fluctuating part of the velocity field to isolate the geometric characteristics of the turbulence from the mean transport. Curvature κ and torsion τ are properties of particle paths in the Frenet–Serret apparatus (Serret, 1851; Frenet, 1852), defined by the tangent $\boldsymbol{T}$, normal $\boldsymbol{N}$, and binormal $\boldsymbol{B}$ unit vectors:

$$\frac{d\boldsymbol{T}}{ds} = \kappa\boldsymbol{N} \qquad \frac{d\boldsymbol{N}}{ds} = -\kappa\boldsymbol{T} + \tau\boldsymbol{B} \qquad \frac{d\boldsymbol{B}}{ds} = -\tau\boldsymbol{N} \tag{1}$$

Here, ds is the path element along the particle trajectory. Curvature measures the path's deviation from a straight line, while torsion describes its deviation from a planar path. Curvature and torsion can be expressed in terms of the fluctuating velocity $\boldsymbol{u}$, acceleration $\boldsymbol{a}$, and jerk $\dot{\boldsymbol{a}}$ as follows:

$$\kappa = \frac{|\boldsymbol{u}\times\boldsymbol{a}|}{|\boldsymbol{u}|^3} \qquad \tau = \frac{\boldsymbol{u}\cdot(\boldsymbol{a}\times\dot{\boldsymbol{a}})}{(\boldsymbol{u}\cdot\boldsymbol{u})^3\kappa^2} \tag{2}$$

Here, $\boldsymbol{u} = (u_1, u_2, u_3)$ represents the fluctuating part of the velocity vector with components in the downstream, vertical, and cross-stream directions, respectively, $\boldsymbol{a} = \dot{\boldsymbol{u}}$ is the Lagrangian acceleration, and $\dot{\boldsymbol{a}}$ is the jerk (the substantial time derivative of the acceleration vector).

Previous work has extensively characterized the curvature and torsion properties in turbulent flows (see, e.g., Braun *et al.*, 2006; Xu *et al.*, 2007). In the canonical case of homogeneous isotropic turbulence, these geometric descriptors are linked to the deformation and stretching of material elements (Girimaji & Pope, 1990). Specifically, the evolution of a material line's curvature is governed by the competition between strain-induced stretching and vorticity-induced rotation. Furthermore, studies in homogeneous isotropic turbulence have shown that these quantities exhibit characteristic pdfs with universal power-law tails, specifically $P(\kappa) \sim \kappa^{-2.5}$ and $P(\tau) \sim \tau^{-3}$ for large values of curvature and torsion, respectively. For small values, the statistics also follow distinct scaling laws: the curvature pdf typically increases as $P(\kappa) \sim \kappa$, while the torsion pdf remains finite and nearly constant as $\tau \to 0$ (Hengster *et al.*, 2024).

More recently, research has shifted toward anisotropic turbulent flows (Alards *et al.*, 2017). Curvature and torsion have been utilized to characterize the geometric statistics of turbulent superstructures in boundary layers (Bross *et al.*, 2023), while curvature-based analysis has been proposed to reveal flow regime changes and spectral features in complex convective environments (Mommert *et al.*, 2025). The impact of large-scale coherent structures on these Lagrangian metrics continues to be a subject of active research (e.g., Hengster *et al.*, 2024).

The aim of the current work is to provide a quantitative analysis of the impact of flow anisotropy on curvature and torsion statistics specifically within homogeneous turbulent shear flow. By isolating the fluctuating velocity components in a constant shear environment, this study provides a direct comparison to the established isotropic scaling laws and clarifies how mean shear modulates the geometric measures of curvature and torsion at different scales of the turbulent motion.

SIMULATION METHOD

In this section, the numerical approach and the wavelet-based, scale-dependent decomposition of the simulation results are introduced.

Numerical Approach

The spatial domain is defined by Cartesian coordinates $\boldsymbol{x} = (x,y,z) = (x_1,x_2,x_3)$, corresponding to the downstream, vertical, and spanwise directions, respectively. The mean velocity field is denoted by $\boldsymbol{U} = (U,V,W)$, where the downstream component is characterized by a prescribed uniform vertical gradient, $S = \partial U/\partial y$:

$$U = Sy \qquad V = W = 0 \tag{3}$$

The numerical framework is based on the incompressible Navier–Stokes equations. This formulation yields the following governing equations for the fluctuating velocity components $\boldsymbol{u} = (u,v,w) = (u_1,u_2,u_3)$ and the fluctuating pressure p:

$$\nabla \cdot \boldsymbol{u} = 0 \tag{4}$$

$$\frac{\partial \boldsymbol{u}}{\partial t} + \boldsymbol{u} \cdot \nabla \boldsymbol{u} + Sy\frac{\partial \boldsymbol{u}}{\partial x} + Sv\boldsymbol{e}_x = -\frac{1}{\rho_0}\nabla p + \nu \nabla^2 \boldsymbol{u} \tag{5}$$

In this formulation, ρ_0 denotes the fluid density and ν represents the kinematic viscosity. The downstream orientation is defined by the unit vector $\boldsymbol{e}_x$.

The governing equations are solved in a coordinate system that translates with the mean flow, following the transformation proposed by Rogallo (1981). This approach facilitates the use of periodic boundary conditions for the fluctuating velocity fields and pressure. Spatial discretization is achieved through a spectral collocation method, while time integration is performed using a fourth-order Runge–Kutta scheme. The numerical simulations are conducted within a cubic domain of dimensions $L_0^3 = (2\pi)^3$ resolved by 512^3 grid points.

The initial flow field is derived from a precursor simulation of isotropic turbulence. This auxiliary simulation was initialized with random fluctuations characterized by a Saffman spectrum with $E(k) \sim k^2$ at low wavenumbers (Saffman, 1967). To permit the development of large-scale structures, the energy density peak was centered at $k = 13$. The isotropic field was evolved for approximately one eddy-turnover time and the k^2 dependence at small wave numbers was maintained. The resulting flow field yielded a Taylor-microscale Reynolds number of $Re_\lambda = q\lambda/\nu = 102$ and a shear number of $SK/\varepsilon = 2$ was imposed. In these definitions, $q = \langle u_i u_i \rangle^{1/2}$ represents the intensity of the velocity fluctuations, $K = q^2/2$ is the turbulent kinetic energy, and $\varepsilon = \nu\langle(\partial u_i/\partial x_k)(\partial u_i/\partial x_k)\rangle$ denotes the dissipation rate. The operator $\langle\cdot\rangle$ signifies a volume average at a fixed time, which is the appropriate ensemble surrogate for these homogeneous flows. For more details see Jacobitz & Schneider (2025).

Wavelet-Based Scale-Dependent Decomposition

A three-dimensional orthogonal vector-valued wavelet decomposition is used to define scale-dependent statistics of different flow quantities. For reviews on wavelets in fluid mechanics we refer to Farge (1992) as well as Schneider & Vasilyev (2010). We consider a generic vector field, e.g., velocity, $\boldsymbol{u} = (u_1,u_2,u_3)$ at a fixed time instant and decompose each vector component $u_\alpha(\boldsymbol{x})$ into an orthogonal wavelet series,

$$u_\alpha(\boldsymbol{x}) = \sum_\lambda \widetilde{u}_\lambda^\alpha \, \psi_\lambda(\boldsymbol{x}). \tag{6}$$

The wavelet coefficients are given by the scalar product $\widetilde{u}^\alpha = \langle u_\alpha, \psi_\lambda \rangle$ (e.g., Farge & Schneider, 2015). The wavelets ψ_λ with the multi-index $\lambda = (l, \boldsymbol{i}, d)$ are well localized functions in scale $L_0 2^{-l}$ (where L_0 corresponds to the size of the computational domain), around position $L_0 \boldsymbol{i}/2^l$, and orientated in one of the seven directions $d = 1,...,7$, respectively. The three components u_α at scale $L_0 2^{-l}$ can be reconstructed by summing only over the position $\boldsymbol{i}$ and direction d indices in eq. (6). The result yields the vector field $\boldsymbol{u}^l$ at scale $L_0 2^{-l}$. Summing all scale contributions yields the total vector field, $\boldsymbol{u} = \sum_l \boldsymbol{u}^l$, as the $\boldsymbol{u}^l$ are mutually orthogonal.

The scale-dependent statistical moments of different flow fields, e.g., curvature in equation 2 or the Reynolds stress anisotropy tensor, can thus be computed from $\boldsymbol{u}^l$ using classical statistical estimators.

RESULTS

The results are first shown for the total flow fields and then for the scale-dependent flow contributions.

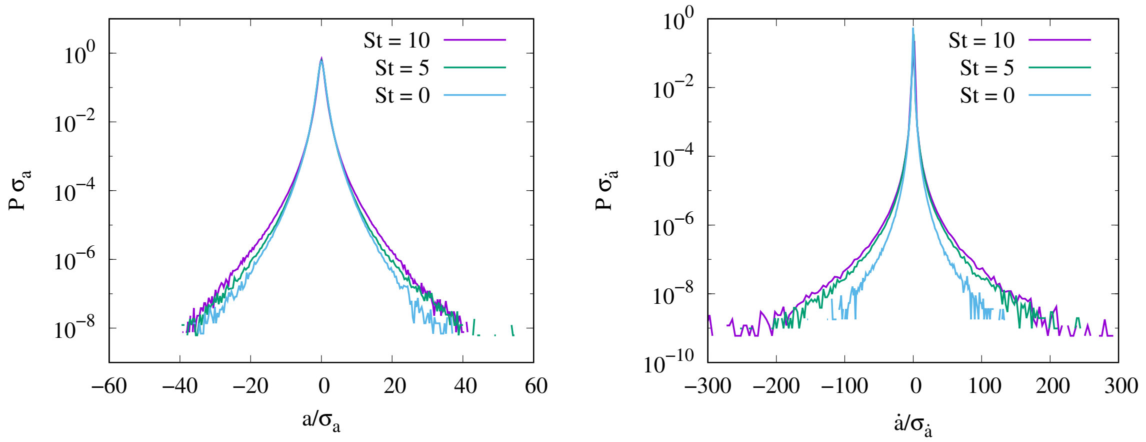

Figure 1. Pdfs of Lagrangian acceleration (left), and jerk (right) at $St = 0$ (corresponding to isotropic turbulence), $St = 5$, and $St = 10$ (corresponding to developed homogeneous turbulent shear flow).

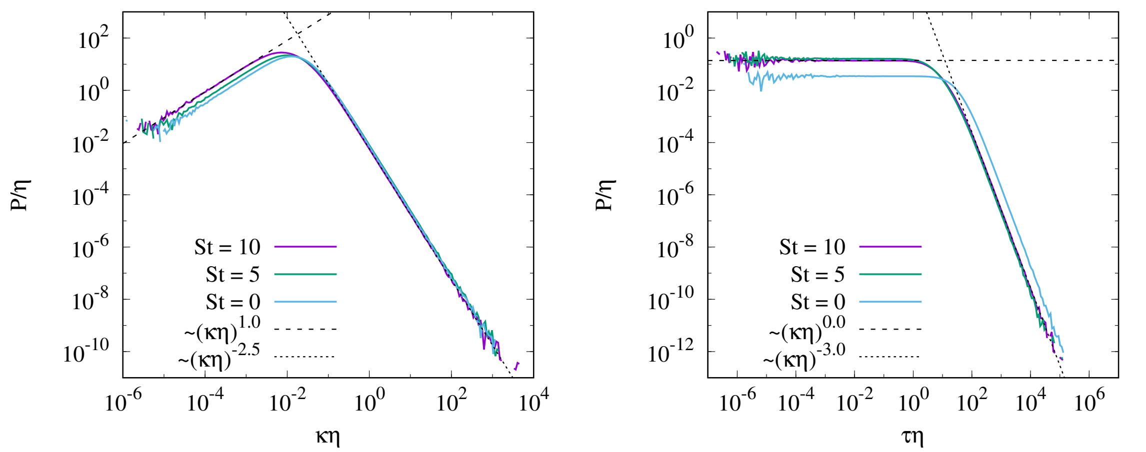

Figure 2. Pdfs of curvature magnitude (left) and torsion magnitude (right) at $St = 0$ (corresponding to isotropic turbulence), $St = 5$, and $St = 10$ (corresponding to developed homogeneous turbulent shear flow).

Curvature and Torsion Properties

Figure 1 shows normalized pdfs for Lagrangian acceleration (left) and jerk (right) at non-dimensional times $St = 0$ (corresponding to isotropic turbulence at the start of the simulation), $St = 5$, and $St = 10$ (both corresponding to well-developed anisotropic homogeneous turbulent shear flow). The pdfs are normalized with the variance of the respective quantities. The pdfs of both Lagrangian acceleration and jerk are heavy-tailed and the tails become more pronounced as time progresses and the Reynolds number increases. The development towards heavy tails is more evident during the transition from isotropic turbulence at $St = 0$ to homogeneous turbulent shear flow at $St = 5$, than for the further evolution of the turbulent shear flow from $St = 5$ to $St = 10$. The pdfs of velocity and vorticity (not shown here) were found to have Gaussian and exponential shapes, respectively.

Figure 2 shows pdfs of the curvature magnitude (left) and torsion magnitude (right) normalized with the Kolmogorov scale $\eta = (\nu^3/\varepsilon)^{1/4}$. The pdfs are computed at non-dimensional times $St = 0$ (isotropic turbulence), $St = 5$, and $St = 10$ (both corresponding to homogeneous turbulent shear flow). The curvature pdfs show two distinct tails: the left tails for small values of $\kappa\eta$ scale $\propto (\kappa\eta)^{1.0}$ and the right tails for large values of $\kappa\eta$ scale $\propto (\kappa\eta)^{-2.5}$. Similarly, the torsion pdfs also show two distinct tails: the left tails for small values of $\tau\eta$ are constant and the right tails for large values of $\tau\eta$ scale $\propto (\tau\eta)^{-3}$. This scaling is consistent with previous studies of a variety of turbulent flows with the curvature and torsion statistics computed along Lagrangian particle paths (Braun *et al.*, 2006; Xu *et al.*, 2007; Hengster *et al.*, 2024). As non-dimensional time St progresses, both pdfs show a shift with the probability for small values of curvature and torsion increasing, while the probability of large values of the two quantities decreases. This can be attributed to the development of large-scale structures in the flow with increasing Reynolds number. It was further observed that the curvature magnitude pdfs, but not the torsion magnitude pdfs, collapse using Heisenberg-Yaglom scaling in agreement with Hengster *et al.* (2024) (not shown here).

Figure 3 shows pdfs of the magnitudes of the three components of the curvature vector $\boldsymbol{\kappa} = (\kappa_1, \kappa_2, \kappa_3) = (\boldsymbol{u} \times \boldsymbol{a})/|\boldsymbol{u}|^3$ at $St = 0$ (left, corresponding to isotropic turbulence) and at $St = 10$ (right, corresponding to developed anisotropic homogeneous turbulent shear flow. The purpose of a consideration of the curvature vector components is a qualitative and quantitative investigation of the impact of flow anisotropy on curvature (see Hengster *et al.*, 2024). The pdfs of the curvature vector component magnitude again show two tails: the left tails are constant and the right tail scale $\propto (\kappa_i\eta)^{-2.5}$. For isotropic turbulence, the three pdfs collapse, confirming the isotropic

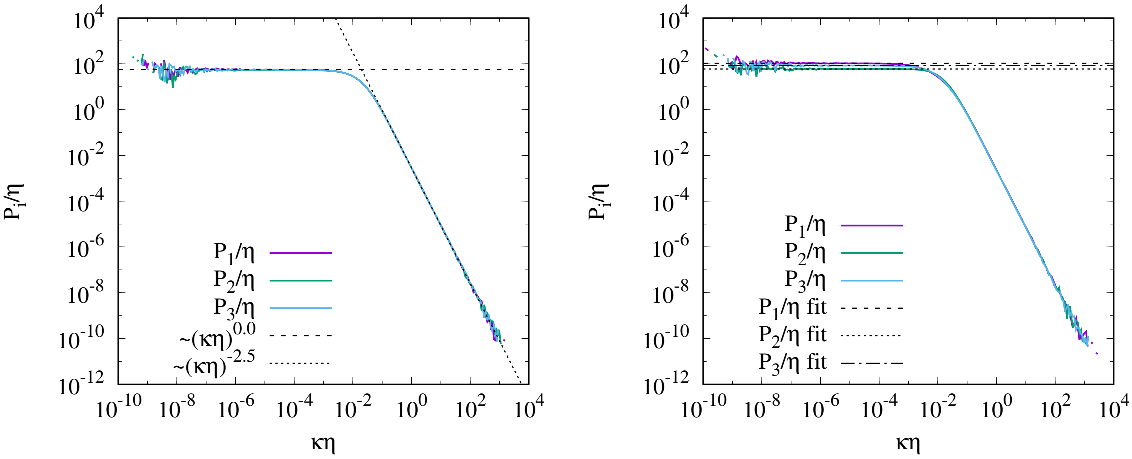

Figure 3. Pdfs of curvature vector component magnitude at $St = 0$ (left, corresponding to isotropic turbulence), and at $St = 10$ (right, corresponding to developed homogeneous turbulent shear flow).

nature of the turbulent flow. For homogeneous turbulent shear flow, however, the left tails show different constant values, $P_1/\eta = 105.322$, $P_2/\eta = 59.398$, and $P_3/\eta = 84.0653$, representing the impact of the flow's anisotropy on its curvature statistics.

Scale-Dependent Analysis

The analysis of the pdfs of the magnitudes of the three components of the curvature vector is now repeated for the decomposed velocity fields at scale index l. Figure 4 shows the results of the scale-dependent analysis for for scale index $l = 2$ (large scales, top, left), $l = 4$ (top, right), $l = 6$ (bottom, left), and $l = 8$ (small scales, bottom, right) for homogeneous turbulent shear flow at $St = 10$. The inserts show the pdfs for small values of the curvature on a linear scale to more clearly indicate the observed differences between the three curvature vector component magnitudes. As the scale index l increases (and the scale of the turbulent motion decreases), the pdfs show two trends: First, the probability of small values of curvature decreases, while the probability of large values increases. Second, the anisotropy of the three curvature vector component magnitude decreases, which will be analyzed in more detail next.

The effects of flow anisotropy are reflected in the constant left tails of the pdfs, while the right tails collapse and show a scaling $\propto (\kappa_i^l \eta)^{-2.5}$. In order to consider the anisotropy effects on the left constant tails of the curvature vector component magnitude pdfs quantitatively, normalized components of the curvature vector are introduced and evaluated for the total flow field

$$p_i = \frac{P_i}{P_1 + P_2 + P_3} - \frac{1}{3} \tag{7}$$

and, correspondingly, for the scale-dependent decomposed flow fields

$$p_i^l = \frac{P_i^l}{P_1^l + P_2^l + P_3^l} - \frac{1}{3} \tag{8}$$

Figure 5 (left) shows the dependence of the normalized components p_i^l at different scales of the turbulent motion with scale index l (open symbols), as well as their values p_i determined for the total flow field (solid symbols) at $St = 0$ (top, corresponding to isotropic turbulence) and $St = 10$ (bottom, corresponding to homogeneous turbulent shear flow). For isotropic turbulence, with almost identical curvature statistics in the different coordinate directions, all components remain small with $p_i^l \approx 0$. For homogeneous turbulent shear flow, however, it is observed that the strongest anisotropy is obtained for the larger scales of the turbulent motion with smaller values of the scale indices l. The anisotropy for the larger scales of the turbulent motion is higher than that for the total fields. Lower, but non-zero levels of anisotropy are observed for the smaller scales of the turbulent motion with larger scale indices l. Please note that the results for scale indices $l = 0$ and 1 are based on low numbers of wavelet modes and the corresponding statistics are not fully converged.

The anisotropy of turbulent flows is often quantified using the Reynolds stress anisotropy tensor b_{ij}:

$$b_{ij} = \frac{\langle u_i u_j \rangle}{\langle u_k u_k \rangle} - \frac{1}{3}\delta ij \tag{9}$$

Here, δ_{ij} is the Kronecker delta. This analysis can also be extended to the decomposed velocity fields at scale index l:

$$b_{ij}^l = \frac{\langle u_i^l u_j^l \rangle}{\langle u_k^l u_k^l \rangle} - \frac{1}{3}\delta ij \tag{10}$$

The scale-dependent components b_{ij}^l are shown in figure 5 (right, reproduced from Jacobitz & Schneider (2025)). A comparison shows that the anisotropy features determined from the pdfs of the curvature vector component magnitude directly follow the diagonal components of the Reynolds shear stress anisotropy tensor. This observation indicates the immediate effect of large-scale, coherent vortices present in homogeneous turbulent shear on the geometrical statistics of fluid particle paths.

SUMMARY

The transition from initial isotropic conditions to a developed homogeneous turbulent shear flow is characterized by an increasing intermittency in the Lagrangian acceleration and

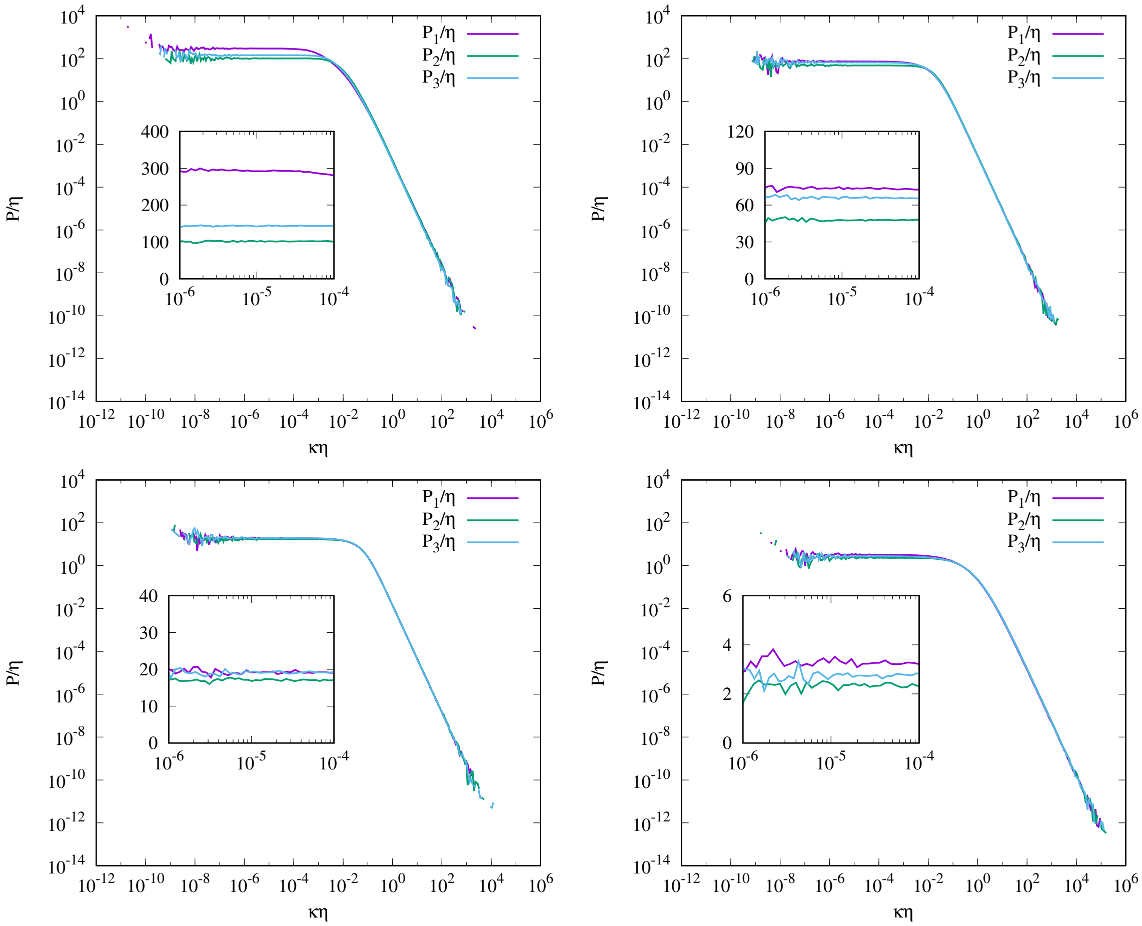

Figure 4. Scale-dependent pdfs of curvature vector component magnitude at $St = 10$ for scale index $l = 2$ (top, left), $l = 4$ (top, right), $l = 6$ (bottom, left), and $l = 8$ (bottom, right).

jerk, manifested by the emergence of increasingly heavy-tailed pdfs as the Reynolds number increased. While the universal scaling laws for large values of curvature ($P(\kappa) \sim \kappa^{-2.5}$) and torsion ($P(\tau) \sim \tau^{-3}$) remain remarkably robust across the shear-driven evolution, the underlying anisotropy of the flow is distinctly encoded in the small-value limit of these geometric statistics. In this regime, the curvature PDF maintains a linear scaling $\propto \kappa^{1.0}$, whereas the torsion PDF remains approximately constant. Through a multi-scale wavelet decomposition, we have demonstrated that this geometric anisotropy is most prominent within the large-scale structures of the motion, where the directional saturation levels of the curvature vector components align closely with the diagonal elements of the Reynolds stress anisotropy tensor. These results provide a quantitative link between the global energetic state of the flow and the local topological evolution of particle paths, suggesting that the structural skeleton of anisotropic turbulence is fundamentally shaped by the persistence of large-scale coherent vortices.

ACKNOWLEDGEMENTS

FGJ acknowledges support fom an International Opportunity Grant from the University of San Diego and the hospitality at Aix-Marseille Université. KS acknowledges funding from the Agence Nationale de la Recherche (ANR), grant CVS-FIT (ANR-23-CE46-0014). We thank Y. Hengster and M. Linkmann for fruitful discussions.

REFERENCES

Alards, K. M. J., Rajaei, H., Del Castello, L., Kunnen, R. P. J., Toschi, F. & Clercx, H. J. H. 2017 Geometry of tracer trajectories in rotating turbulent flows. *Phys. Rev. Fluids* **2** (4), 044601.

Braun, W., De Lillo, F. & Eckhardt, B. 2006 Geometry of particle paths in turbulent flows. *J. Turbul.* (7), N62.

Bross, M., Schanz, D., Novara, M., Eich, F., Schröder, A. & Kähler, C. J. 2023 Turbulent superstructure statistics in a turbulent boundary layer with pressure gradients. *Eur. J. Mech. B Fluids* **101**, 209–218.

Duplat, J. & Villermaux, E. 2008 Mixing by random stirring in confined mixtures. *J. Fluid Mech.* **617**, 51–86.

Farge, M. 1992 Wavelet transforms and their applications to turbulence. *Annu. Rev. Fluid Mech.* **24** (1), 395–458.

Farge, M. & Schneider, K. 2015 Wavelet transforms and their applications to MHD and plasma turbulence: a review. *J. Plasma Phys.* **81** (6), 435810602.

Franzese, P. 2003 Lagrangian stochastic modeling of a fluctuating plume in the convective boundary layer. *Atmos. Environ.* **37** (12), 1691–1701.

Frenet, F. 1852 Sur les courbes à double courbure. *J. Math. Pures Appl.* **17**, 437–447.

Girimaji, S. S. & Pope, S.B. 1990 Material-element deformation in isotropic turbulence. *J. Fluid Mech.* **220**, 427–458.

Hengster, Y., Lellep, M., Weigel, J., Bross, M., Bosbach, J., Schanz, D., Schröder, A., Huhn, F., Novara, M., Garaboa Paz, D., Kähler, C.J. & Linkmann, M. 2024 Effects of anisotropy on the geometry of tracer particle trajectories in

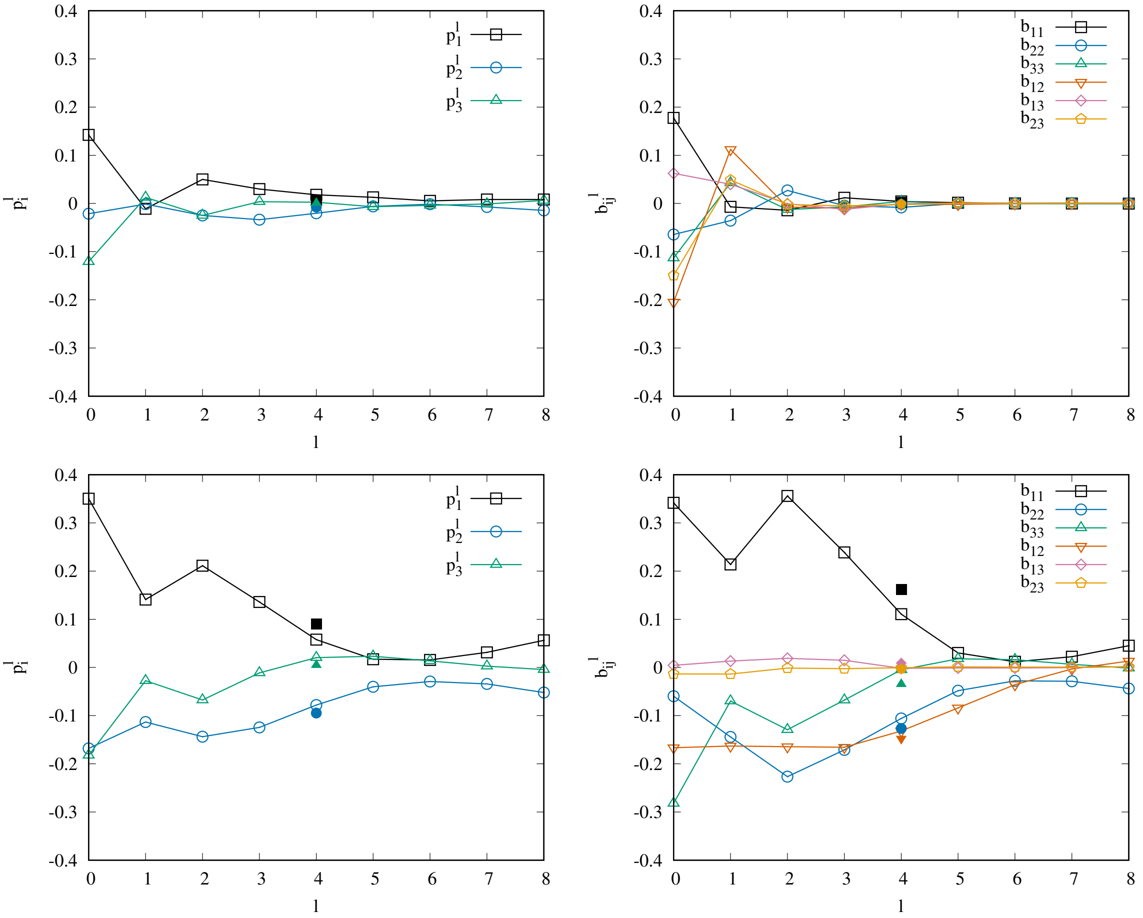

Figure 5. Scale-dependent normalized components of the curvature vector (left) and scale-dependent components of the Reynolds stress anisotropy tensor (right) for homogeneous turbulent shear flow for isotropic turbulence at $St = 0$ (top) and for developed homogeneous turbulent shear flow at $St = 10$ (bottom).

turbulent flows. *Eur. J. Mech. B Fluids* **103**, 284–298.

Jacobitz, F. G. & Schneider, K. 2021 Lagrangian and Eulerian accelerations in turbulent stratified shear flows. *Phys. Rev. Fluids* **6** (7), 074609.

Jacobitz, F. G. & Schneider, K. 2025 Scale-dependent analysis of the return to isotropy from anisotropic homogeneous turbulent shear flows originating from Batchelor and Saffman turbulence. *Int. J. Heat Fluid Fl.* **116**, 109927.

Jacobitz, F. G., Schneider, K., Bos, W. J. T. & Farge, M. 2016 Structure of sheared and rotating turbulence: Multiscale statistics of Lagrangian and Eulerian accelerations and passive scalar dynamics. *Phys. Rev. E* **93** (1), 013113.

LaCasce, J.H. 2008 Statistics from Lagrangian observations. *Prog. Oceanogr.* **77** (1), 1–29.

Meneveau, C. & Katz, J. 2000 Scale-invariance and turbulence models for large-eddy simulation. *Annu. Rev. Fluid Mech.* **32** (1), 1–32.

Minier, J.-P. & Peirano, E. 2001 The pdf approach to turbulent polydispersed two-phase flows. *Phys. Rep.* **352** (1-3), 1–214.

Mommert, M., Bahavar, P., Barta, R., Bauer, C., Volk, M.-C. & Wagner, C. 2025 Curvature-based energy spectra revealing flow regime changes in Rayleigh-Bénard convection. *Eur. J. Mech. B Fluids* p. 204343.

Pope, S. B. 1994 Lagrangian pdf methods for turbulent flows. *Annu. Rev. Fluid Mech* **26** (1), 23–63.

Rogallo, R. S. 1981 Numerical experiments in homogeneous turbulence. Technical Report TM 81315. NASA Ames Research Center, Moffett Field, CA, United States.

Saffman, P. G. 1967 The large-scale structure of homogeneous turbulence. *J. Fluid Mech.* **27** (3), 581–593.

Schneider, K. & Vasilyev, O. V. 2010 Wavelet methods in computational fluid dynamics. *Annu. Rev. Fluid Mech.* **42**, 473–503.

Serret, J.-A. 1851 Sur quelques formules relatives à la théorie des courbes à double courbure. *J. Math. Pures Appl.* **16**, 193–207.

Toschi, F. & Bodenschatz, E. 2009 Lagrangian properties of particles in turbulence. *Annu. Rev. Fluid Mech.* **41** (1), 375–404.

Xu, H., Ouellette, N. T. & Bodenschatz, E. 2007 Curvature of Lagrangian trajectories in turbulence. *Phys. Rev. Lett.* **98** (5), 050201.

Yeung, P. K. 2002 Lagrangian investigations of turbulence. *Annu. Rev. Fluid Mech.* **34** (1), 115–142.